CRYSTAL GROWTH & DESIGN

Article

pubs.acs.org/crystal

Synthesis, Structures, Polymorphism, and Magnetic Properties of Transition Metal Thiocyanato Coordination Compounds

Susanne Wöhlert,[†] Tomče Runčevski,[§] Robert E. Dinnebier,[§] Stefan G. Ebbinghaus,[‡] and Christian Näther*,[†]

[†]Institut für Anorganische Chemie, Christian-Albrechts-Universität zu Kiel, Max-Eyth-Straße 2, 24118 Kiel, Germany

[§]Max-Planck Institute for Solid State Research, Heisenbergstraße 1, 70569 Stuttgart, Germany

[‡]Martin-Luther-Universität Halle-Wittenberg, Institut für Chemie, Kurt-Mothes-Straße 2, 06120 Halle/Saale, Germany

Supporting Information

ABSTRACT: Reaction of manganese, iron, and nickel thiocyanate with 4-ethylpyridine leads to the formation of single crystals of compounds with composition $M(NCS)_2(L)_4$ (**1**), $M(NCS)_2(L)_2(H_2O)_2$ (**2-Mn**), and $M(NCS)_2(L)_2$ (**3**) with M = Mn, Fe, and Ni and L = 4-ethylpyridine. For most compounds, different polymorphic modifications are observed, and their transition behavior and thermodynamic stability was investigated. Additionally, compounds of composition $M(NCS)_2(L)_2$ (M = Mn or Ni) were prepared from solution and by thermal decomposition of compounds **1** and **2**, which lead to different stable and metastable modifications. The crystal structures of most compounds were determined by single crystal X-ray diffraction and some of them by Rietveld refinements. Compounds **1** and **2** consist of octahedrally coordinated discrete complexes with terminal N-bonded thiocyanato anions. In compounds **3**, the metal cations are linked by pairs of μ-1,3-bridging thiocyanato anions into chains. Surprisingly, thermal decomposition of $Ni(NCS)_2(4\text{-ethylpyridine})_4$ leads to the formation of a new compound of composition $Ni(NCS)_2(4\text{-ethylpyridine})$ (**4-Ni**). Magnetic measurements reveal that **3-Mn/II** and **3-Mn/III** show antiferromagnetic ordering at T_N = 21.5 and 23.9 K and that **4-Ni** is a metamagnet with a critical field of 1.4 kOe at 2 K. All other compounds show Curie or Curie–Weiss behavior with no magnetic anomalies.

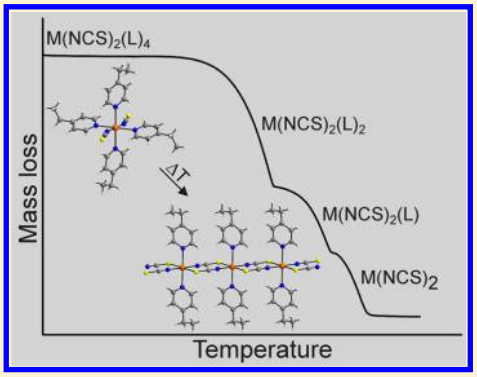

INTRODUCTION

Recently, investigations on new synthetic routes for novel coordination compounds, inorganic–organic hybrid materials, and metal–organic frameworks with desired physical properties stand at the frontiers of inorganic chemistry research.[1−9] For that purpose, different strategies for a rational design of specific structures need to be developed, and structure–property relationships need to be investigated in detail.[10−20] Besides the chemical synthesis itself, a major issue is governing the formation of a desired polymorph (or isomer), since polymorphism is a usual feature of coordination compounds.[21−32] In this context, special attention should be paid to the phase transition within different polymorphs, the way in which they can be crystallized in pure form, and their relative stability, that is to find the thermodynamically stable forms.[23−27]

Concerning the physical properties of coordination compounds, materials showing cooperative magnetic phenomena are of special interest. Those phenomena can emerge when paramagnetic transition metal atoms are linked by neutral or anionic ligands, which can mediate magnetic exchange interactions.[33−42] Within the scope of our ongoing investigations on the magnetic properties of coordination compounds based on transition metal thio- and selenocyanates, we synthesized a number of different materials. Some of them, together with selected examples from the literature are given in the reference list.[43−58] However, the preparation of such compounds in which the metal cations are linked by bridging anionic ligands is sometimes difficult to achieve if the synthesis is performed in solution. Therefore, we have developed an alternative, solid-state route based on thermal decomposition of suitable precursors.[59−61] It should be noted that preparation of coordination compounds by solid state methods is not uncommon and different methods were reported.[62−68] Given that our aim is building up a thio- and selenocyanate bonded network of metal cations, we decided to start with complexes where the metal cations are octahedrally coordinated by four neutral N-donor coligands and two terminal N-bonded thio- or selenocyanato anions. Upon heating, the coligands are removed in a stepwise fashion, and in most cases, the octahedral coordination is retained during ligand removal, which enforces the formation of desired samples in which the metal cations are linked by μ-1,3-bridging anionic ligands. The new materials are obtained in quantitative yield, in most cases as single phases and sometimes as polymorphic modifications.[23,26,27,61] As

Received: January 8, 2014
Revised: February 12, 2014
Published: March 5, 2014

   dx.doi.org/10.1021/cg500037d | *Cryst. Growth Des.* 2014, 14, 1902–1913

expected, most of them exhibit cooperative magnetic phenomena, including metamagnetic behavior.[69−75] Within this project, for example, 1D-linked samples of composition $M(NCS)_2(pyridine)_2$ (M = Mn, Fe, Co, or Ni) were investigated. The Mn compound was shown to be an antiferromagnet, while the Fe and Ni analogues are metamagnets, and for the Co containing sample, a slow relaxation of the magnetization was observed.[75,76] To determine whether this interesting magnetic behavior is retained on ligand exchange, we prepared $Co(NCS)_2$(4-ethylpyridine)$_2$. This material exhibits a very similar structure to that of $Co(NCS)_2(pyridine)_2$ but is a metamagnet that shows metamagnetism and slow relaxations below and above the critical field.[77] Motivated by this finding and in order to study the influence of the metal cation, we focused on 4-ethylpyridine as ligand. To the best of our knowledge only $Ni(NCS)_2(4\text{-ethylpyridine})_4$ existing in two polymorphs (**1-Ni/I** and **1-Ni/II**) is reported in the literature.[78] Additionally, some solvates of $Ni(NCS)_2(4\text{-ethylpyridine})_4$ are also reported.[78]

Accordingly, various materials crystallizing in different polymorphic modifications were prepared and structurally characterized by single crystal X-ray diffraction and by Rietveld refinements (Table 1). Interestingly, we obtained an unusual ligand-deficient compound of composition $[Ni(NCS)_2(4\text{-ethylpyridine})]_n$ (**4-Ni**), which shows metamagnetic behavior.

Table 1. Compounds Investigated in This Work[a]

compound	space group
$M(NCS)_2(L)_4$ (L = 4-ethylpyridine)	
$Ni(NCS)_2(4\text{-ethylpyridine})_4$ (**1-Ni/I**)	$P\bar{1}$
$Ni(NCS)_2(4\text{-ethylpyridine})_4$ (**1-Ni/II**)	$P\bar{1}$
$Mn(NCS)_2(4\text{-ethylpyridine})_4$ (**1-Mn/II**)	$P\bar{1}$
$Mn(NCS)_2(4\text{-ethylpyridine})_4$ (**1-Mn/III**)	$P2_1/c$
$Mn(NCS)_2(4\text{-ethylpyridine})_4$ (**1-Mn/IV**)	$P\bar{1}$
$Fe(NCS)_2(4\text{-ethylpyridine})_4$ (**1-Fe/I**)	$P\bar{1}$
$Fe(NCS)_2(4\text{-ethylpyridine})_4$ (**1-Fe/II**)	$P\bar{1}$
$Mn(NCS)_2(4\text{-ethylpyridine})_2(H_2O)_2$ (**2-Mn**)	$P2_1/c$
$M(NCS)_2(L)_2$	
$Ni(NCS)_2(4\text{-ethylpyridine})_2$ (**3-Ni/I**)	$P\bar{1}$
$Ni(NCS)_2(4\text{-ethylpyridine})_2$ (**3-Ni/II**)	Cc
$Mn(NCS)_2(4\text{-ethylpyridine})_2$ (**3-Mn/II**)	Cc
$Mn(NCS)_2(4\text{-ethylpyridine})_2$ (**3-Mn/III**)	$P2_1/c$
$Fe(NCS)_2(4\text{-ethylpyridine})_2$ (**3-Fe/II**)	Cc
$M(NCS)_2(L)$	
$Ni(NCS)_2(4\text{-ethylpyridine})$ (**4-Ni**)	

[a]Identical roman numerals correspond to isotypic modifications; thus some numbers are missing. The crystal structure of **4-Ni** remains unknown.

EXPERIMENTAL SECTION

Materials and General Methods. All chemicals and solvents were used without further purification. $NiCl_2{\cdot}6H_2O$, $FeSO_4{\cdot}7H_2O$, KNCS, $MnSO_4{\cdot}2H_2O$, $Ba(NCS)_2{\cdot}3H_2O$, and 4-ethylpyridine were obtained from Alfa Aesar. $Mn(NCS)_2$ was prepared by a reaction of equimolar amounts of $MnSO_4{\cdot}2H_2O$ and $Ba(NCS)_2{\cdot}3H_2O$ in water. The resulting precipitate of $BaSO_4$ was filtered off, and the filtrate was evaporated to complete dryness resulting in a white residue of $Mn(NCS)_2$. The desired complexes (see Results and Discussion) were prepared by stirring different molar ratios of the reactants for 3 days. The residues obtained were filtered off, washed with water and diethyl ether, and dried in vacuum.

Elemental Analysis. All synthesized samples were investigated by CHNS analysis using a EURO EA elemental analyzer (EURO VECTOR Instruments).

X-ray Powder Diffraction (XRPD). The measurements were performed using (1) a PANalytical X'Pert Pro MPD reflection diffractometer with Cu Kα radiation equipped with a PIXcel semiconductor detector and (2) a Stoe transmission powder diffraction system (STADI-P) with Cu Kα radiation that is equipped with a linear position-sensitive detector. The data collection of the patterns used for Rietveld refinement was performed on high-resolution powder diffractometer Bruker D8 Advance with Ge(111)-Johanson-type monochromator and VÅNTEC-1 position sensitive detector in Debye−Scherrer geometry.

Rietveld Refinements. The Rietveld refinements were performed using the program suite TOPAS 4.2, and selected crystallographic data are listed in Table 2.[79] The following overall parameters were subjected to refinement: phase scale factor, background coefficients (Chebyshev polynomials of order smaller than 10), unit cell parameters, zero-error shift, and parameters for the strain contribution. The displacement factors were treated isotropically. Despite the use of capillaries in Debye−Scherrer geometry, a small amount of the preferred orientation was detected and was adequately described by the use of symmetry-adapted spherical harmonics. The metal cations were allowed to move freely, while for the ligands rigid bodies were created and their x, y, z fractional positions, together with bond distances, angles, and torsions were refined.

Table 2. Details on the Rietveld Refinement for Compounds 3-Mn/II and 3-Fe/II

	3-Mn/II	3-Fe/II
formula	$C_{16}H_{18}MnN_4S_2$	$C_{16}H_{18}FeN_4S_2$
MW, g·mol^{-1}	385.40	386.32
cryst syst	monoclinic	monoclinic
space group	Cc	Cc
a, Å	11.488(4)	11.365(7)
b, Å	39.84(2)	39.80(3)
c, Å	9.366(3)	9.276(6)
α, deg	90	90
β, deg	114.70(3)	115.09(5)
γ, deg	90	90
V, Å^3	3895.3(9)	3799.9(9)
T, K	293	293
Z	4	4
D_{calc}, mg·m^3	1.252	1.287
θ_{max}, deg	50	50
R_{Bragg}	0.024 17	0.027 95
R_{exp}	0.029 56	0.011 89
R_{wp}	0.0210	0.025 56
R_p	0.024 91	0.019 04
GOF	1.086	2.150

IR Spectroscopy. IR spectroscopy was performed using an ATI Mattson Genesis series FTIR spectrometer.

Differential Thermal Analysis and Thermogravimetry (DTA-TG). The measurements were performed in nitrogen atmosphere (purity 5.0) in Al_2O_3 crucibles using a NETZSCH STA-409CD thermobalance. The instrument was calibrated using standard reference materials. All measurements were performed with a heating rate of 4 K min^{-1} and a low rate of 75 mL min^{-1}.

Differential Scanning Calorimetry. The DSC experiments were performed using a DSC 1 star system with STARe Excellence software from Mettler-Toledo AG.

Magnetic Measurements. All magnetic measurements were performed using a Quantum Design PPMS (Physical Property Measurement System), equipped with a 9 T magnet. The data were corrected for core diamagnetism.

dx.doi.org/10.1021/cg500037d | Cryst. Growth Des. 2014, 14, 1902−1913

Table 3. Selected Crystal Data and Details on the Structure Determination from Single Crystal Data for the Investigated Compounds

	1-Mn/III	1-Mn/IV	1-Fe/I	1-Fe/II	2-Mn	3-Ni/I	3-Ni/II	3-Mn/III
formula	$C_{30}H_{36}MnN_6S_2$	$C_{30}H_{36}MnN_6S_2$	$C_{30}H_{36}FeN_6S_2$	$C_{30}H_{36}FeN_6S_2$	$C_{16}H_{22}MnN_4O_2S_2$	$C_{16}H_{18}N_4NiS_2$	$C_{16}H_{18}N_4NiS_2$	$C_{16}H_{18}MnN_4S_2$
MW, g·mol^{-1}	599.71	599.71	600.92	600.62	421.44	389.17	389.17	385.40
cryst syst	monoclinic	triclinic	triclinic	triclinic	monoclinic	triclinic	monoclinic	monoclinic
space group	$P2_1/c$	$P\bar{1}$	$P\bar{1}$	$P\bar{1}$	$P2_1/c$	$P\bar{1}$	Cc	$P2_1/c$
a, Å	9.8148(3)	11.8301(5)	10.1658(8)	10.3881(4)	11.0253(7)	8.9684(6)	11.1707(8)	5.7737(4)
b, Å	16.9806(7)	16.4075(8)	17.0109(12)	16.3106(7)	12.8112(7)	10.6770(7)	39.5124(19)	18.3907(10)
c, Å	20.0807(6)	18.6847(8)	19.4946(12)	20.1423(8)	7.6416(5)	10.9560(7)	9.1330(7)	8.5647(6)
α, deg	90	72.304(3)	85.379(8)	91.552(3)	90	67.460(5)	90	90
β, deg	99.849(2)	75.684(4)	84.001(8)	90.799(3)	107.476(7)	67.360(5)	115.200(8)	96.165(8)
γ, deg	90	77.015(4)	73.599(8)	102.835(3)	90	83.940(5)	90	90
V, Å^3	3297.3(2)	3303.6(3)	3211.7(4)	3325.6(2)	1029.54(11)	893.21(10)	3647.5(4)	904.16(10)
T, K	293	293	200	293	200	200	200	200
Z	4	4	4	4	2	2	8	2
D_{calc}, mg·m^3	1.208	1.206	1.242	1.200	1.359	1.447	1.417	1.419
μ, mm^{-1}	0.554	0.553	0.628	0.606	0.860	1.323	1.296	0.964
θ_{max}, deg	25.00	25.00	25.00	26.00	27.49	28.00	28.02	27.50
reflns collected	37 729	26 915	20 297	32 009	7560	9813	20 354	9339
unique reflns	5758	11 523	11 011	12 925	2350	4281	8521	2043
R_{int}	0.0503	0.0248	0.0529	0.0639	0.0283	0.0454	0.0391	0.0614
min/max. transm			0.8067/0.9343	0.5318/0.8459	0.7762/0.8776	0.5959/0.8285	0.7714/0.8779	0.7872/0.8988
reflns $[F_0 > 4\sigma(F_0)]$	4509	7819	7764	7999	1963	2603	7390	1726
params	355	733	711	726	118	211	415	106
R_1 $[F_0 > 4\sigma(F_0)]$	0.0663	0.0605	0.0434	0.0777	0.0426	0.0516	0.0383	0.0303
wR_2	0.1656	0.1692	0.1188	0.2237	0.1174	0.1351	0.1043	0.0779
GOF	1.128	1.046	0.981	1.061	1.040	1.040	1.037	1.032
$\Delta\rho_{max/min}$, e·Å^{-3}	0.257/−0.201	0.349/−0.275	0.624/−0.468	0.466/−0.323	0.582/−0.465	0.493/−0.810	0.538/−0.720	0.295/−0.497

dx.doi.org/10.1021/cg500037d | Cryst. Growth Des. 2014, 14, 1902−1913

Single-Crystal Structure Analysis. Data collection was carried out using a two imaging plate diffraction system from Stoe (IPDS-1 for **1-Fe/I**, **2-Mn**, **3-Ni/II**, and **3-Mn/III** and IPDS-2 for **1-Mn/III**, **1-Mn/IV**, **1-Fe/II**, and **3-Ni/I**) using Mo Kα radiation. For some compounds, a numerical absorption correction was performed (see Table 3). The structures were solved with direct methods using SHELXS-97, and structure refinements were performed against F^2 using SHELXL-97.[80] Numerical absorption corrections were applied using X-RED and X-SHAPE of the program package X-Area. Hydrogen atoms were refined with anisotropic displacement parameters. All hydrogen atoms were positioned with idealized geometry and were refined isotropically with $U_{iso}(H) = 1.2U_{eq}(C)$ (1.5 for methyl H atoms) using a riding model. The water H atoms in compound **2-Mn** were located in a difference Fourier map, their bond lengths were set to ideal values, and finally they were refined using a riding model with $U_{iso}(H) = 1.5U_{eq}(O)$. In **1-Mn/IV**, **1-Fe/I**, **1-Fe/II**, **2-Mn**, **3-Ni/I**, and **3-Ni/II**, some C atoms of the ethyl groups are disordered and were refined using a split model. Compound **3-Ni/II** is racemically twinned, and therefore, a twin refinement was performed (BASF parameter = 0.58(2)). Platon does not suggest higher symmetry, and all other attempts to transform the structure in the centrosymmetric space goup fail. Details of the structure determination are given in Table 3.

CCDC 986328 (**1-Mn/III**), CCDC 986329 (**1-Mn/IV**), CCDC 986327 (**1-Fe/I**), CCDC 986326 (**1-Fe/II**), CCDC 986330 (**2-Mn**), CCDC 986332 (**3-Ni/I**), CCDC 986333 (**3-Ni/II**), CCDC 986335 (**3-Mn/II**), CCDC 986331 (**3-Mn/III**), and CCDC 986334 (**3-Fe/II**) contain the supplementary crystallographic data for this paper. These data can be obtained free charge from the Cambridge Crystallographic Data Centre via http://www.ccdc.cam.ac.uk/data_request/cif.

RESULTS AND DISCUSSION

Synthetic Investigations in Solution. In the classical, solution based synthesis, different molar ratios of $M(NCS)_2$ (M = Ni, Mn, or Fe) were reacted with 4-ethylpyridine in water (Table 4), and the residues obtained were investigated by XRPD, elemental analysis, and IR spectroscopy. The procedure was repeated using methanol, ethanol, and acetonitrile, and the results are given in the Supporting Information, Table S1.

Table 4. Crystalline Phases Obtained after 3 Days Stirring of $M(NCS)_2$ (M = Ni, Mn, and Fe) with 4-Ethylpyridine in Water at Room-Temperature

M	1:4	1:2	1:1	2:1	4:1
Ni	**1-Ni/II**	**1-Ni/II**	**3-Ni/II**	**3-Ni/II**	**3-Ni/II**
Mn	**1-Mn/III**	**1-Mn/III**	**2-Mn**	**2-Mn**	**3-Mn/III**
Fe	**1-Fe/II**	**1-Fe/II**	$Fe(NCS)_2$	$Fe(NCS)_2$	$Fe(NCS)_2$

In the cases using coligand rich solution (1:4 and 1:2 ratios), compounds of composition $M(NCS)_2(4\text{-ethylpyridine})_4$ were obtained. The XRPD patterns show that the crystal structures of the Ni and Fe complexes (**1-Ni/II** and **1-Fe/II**) are isotypic to the reported polymorphic modification **1-Ni/II**.[78] The Mn complex, however, gave a different pattern indicating that a further modification (**1-Mn/III**) is formed. For all of these complexes, the value of the asymmetric CN stretching vibration indicated that the thiocyanato anions are terminally N-bonded to the metal cations [$\nu_{as}(CN) = 2066$ cm^{-1} for **1-Ni/II**, 2044 cm^{-1} for **1-Mn/III**, 2047 cm^{-1} for **1-Fe/II** (Supporting Information, Figure S1)]. The Fe cation did not form any complex with the coligand when the ratio of $M(NCS)_2$ and 4-ethylpyridine was 1:1, 2:1, and 4:1. In contrast, the Ni cation reacted in each of the three ratios, giving a complex of composition $Ni(NCS)_2(4\text{-ethylpyridine})_2$ (**3-Ni/II**) with μ-1,3 bridging anionic ligands [$\nu_{as}(CN) = 2112$ cm^{-1} (Supporting Information, Figure S1)]. The Mn cation, in solutions where the $Mn(NCS)_2$ and 4-ethylpyridine ratios were 1:1 and 2:1, formed a aqua complex of a composition $Mn(NCS)_2(4\text{-ethylpyridine})_2(H_2O)_2$ (**2-Mn**) with terminal N-bonded anionic ligands [$\nu_{as}(CN) = 2085$ cm^{-1} (Supporting Information, Figure S1)]. With increasing concentration of the metal salt (4:1 ratio), a 4-ethylpyridine-deficient compound with bridging anionic ligands of composition $Mn(NCS)_2(4\text{-ethylpyridine})_2$ was obtained in the polymorphic modification **III** (**3-Mn/III**) [$\nu_{as}(CN) = 2091$ cm^{-1} (Supporting Information, Figure S1)]. In the other solvents, no further crystalline phases were obtained but in, for example, acetonitrile the aqua complex **2-Mn** cannot be obtained because of the low water content in the solutions (Supporting Information, Table S1).

In further crystallization experiments, single crystals of the coligand rich complexes (**1-Fe/I**, **1-FeII**, **1-Mn/III**, and **1-Mn/IV**), the aqua complex (**2-Mn**), and the 4-ethylpyridine-deficient compounds (**3-Ni/I**, **3-Ni/II**, and **3-Mn/III**) were obtained.

In order to prove the phase purity of the complexes, their XRPD patterns (**1-Ni/II**, **1-Mn/III**, **1-Mn/IV**, **1-FeII**, **2-Mn**, **3-Ni/I**, **3-Ni/II**, and **3-Mn/III**) were collected and compared with patterns simulated from the single crystal structures (Supporting Information, Figure S2). It was proven that all modifications were obtained as single phases, except **1-Mn/III**, which crystallized in a mixture with **1-Mn/IV**, which was not detected in the IR measurements.

Crystal Structure of the Compounds of Composition $M(NCS)_2(4\text{-ethylpyridine})_4$. For the complexes of composition $M(NCS)_2(4\text{-ethylpyridine})_4$, four different crystal structures were observed. Forms **I** and **II** of $Fe(NCS)_2(4\text{-ethylpyridine})_4$ crystallize in the triclinic space group $P\bar{1}$ and are isotypic to **1-Ni/I** and **1-Ni/II**, which were reported several years ago.[78] The asymmetric unit in both modifications consists of two crystallographically independent iron(II) cations, four thiocyanato anions, and eight neutral coligands, all of them situated on a general position (Supporting Information, Figure S3–S4).

The Mn compounds crystallize in two different crystal structures, **III** and **IV**. Form **1-Mn/III** crystallizes in the monoclinic space group $P2_1/c$, where the asymmetric unit consists of two crystallographically independent manganese(II) cations located on centers of inversion, two thiocyanato anions, and four 4-ethylpyridine ligands that occupy general positions (Supporting Information, Figure S5). Form **1-Mn/IV** crystallizes in space group $P\bar{1}$, with four formula units in the unit cell and three crystallographically independent Mn(II) cations, two of them located on centers of inversion (Supporting Information, Figure S6). In all compounds, the metal cations are coordinated by two N-bonded thiocyanato anions and four 4-ethylpyridine ligands building slightly distorted octahedra (Figure 1, left).

The M–N distances range from 2.085(2) to 2.346(3) Å and are comparable to those in similar compounds (Supporting Information, Table S2–S5). The differences in the crystal structures are predominantly found in the arrangement of the discrete complexes in the crystal structure (Supporting Information, Figures S7–S8).

Crystal Structure of $Mn(NCS)_2(4\text{-ethylpyridine})_2(H_2O)_2$. Compound **2-Mn** crystallizes in the monoclinic space group $P2_1/c$ with two formula units in the unit cell. The asymmetric unit consists of one manganese(II) cation, which is located on a center of inversion, one thiocyanato anion, one 4-

dx.doi.org/10.1021/cg500037d | Cryst. Growth Des. 2014, 14, 1902–1913

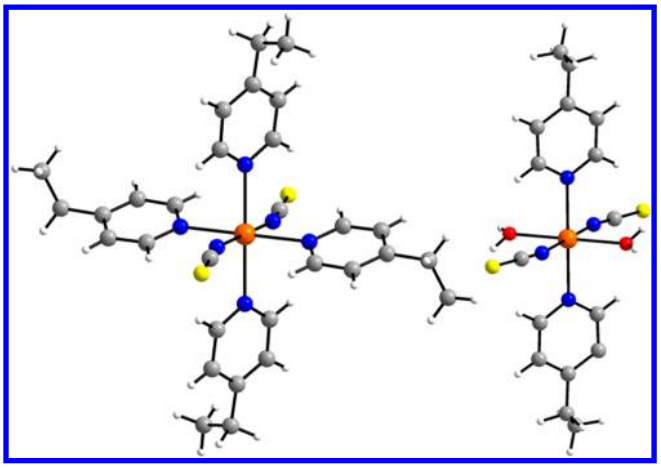

Figure 1. Coordination around the metal cation in the crystal structures of **1-Mn/III** (left) and **2-Mn** (right). Color code: orange = metal; blue = nitrogen; yellow = sulfur; red = oxygen; gray = carbon; white = hydrogen. ORTEP plots of all compounds can be found in the Supporting Information, Figures S3–S6 and S9.

ethylpyridine ligand, and one water molecule, located on a general position (Supporting Information, Figure S9). In the crystal structure, discrete complexes are found in which the Mn cations are coordinated by two N-bonded thiocyanato anions, two 4-ethylpyridine ligands, and two water molecules within a slightly distorted octahedral geometry. The Mn–N and Mn–O distances range from 2.189(2) to 2.2626(19) Å, and the angles are 84.93(8)°, 95.07(8)°, and 180° (Supporting Information, Table S6). In the crystal structure, the discrete complexes are connected by intermolecular OH···S hydrogen bonding with H···S distances of 2.525 and 2.515 Å (Supporting Information, Figure S10).

Crystal Structures of the Compounds of Composition $M(NCS)_2(4\text{-ethylpyridine})_2$. Compound **3-Ni/I** crystallizes in the triclinic space group $P\bar{1}$ with two formula units in the unit cell. The asymmetric unit consists of two crystallographically independent nickel(II) cations located on centers of inversion, two thiocyanato anions, and two 4-ethylpyridine ligands located on a general position (Supporting Information, Figure S11). Polymorph **3-Ni/II** crystallizes in the monoclinic space group *Cc* with eight formula units in the unit cell. The asymmetric unit consists of two crystallographically independent nickel(II) cations, four thiocyanato anions, and four 4-ethylpyridine ligands all situated on a general position (Supporting Information, Figure S12). Significant differences between the two Ni modifications are found in the packing of the chains. In **3-Ni/I**, they are arranged in layers, whereas in **3-Ni/II**, a typical sandwich-herringbone arrangement is found, similar to that in **3-Mn/III** (Supporting Information, Figure S13).

Compound **3-Mn/III** crystallizes in the monoclinic space group $P2_1/c$ with two formula units in the unit cell. The asymmetric unit consists of one manganese(II) cation located on a center of inversion, one thiocyanato anion, and one 4-ethylpyridine ligand on general positions (Supporting Information, Figure S14). In the crystal structure, each metal(II) cation is coordinated by two N-bonded and two S-bonded thiocyanato anions, as well as two *trans*-coordinated 4-ethylpyridine ligands in a slightly distorted octahedral geometry (Figure 2).

The M–N and M–S distances ranges from 2.033(3) to 2.7381(4) Å with angles around the metal(II) cations between

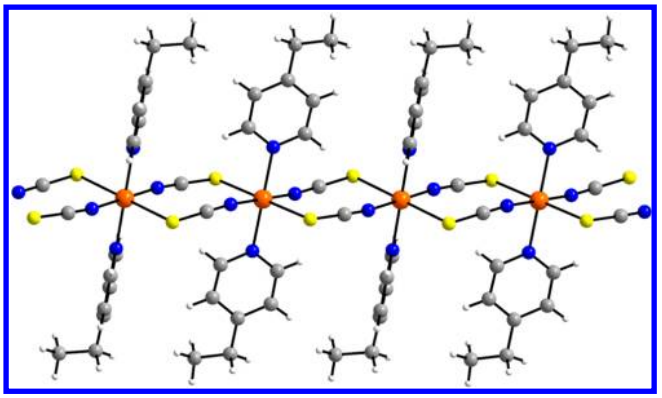

Figure 2. Fragment of one chain in the crystal structure of **3-Ni/I**. Color code: orange = metal; blue = nitrogen; yellow = sulfur; gray = carbon; white = hydrogen). ORTEP plots of all 1:2 compounds can be found in the Supporting Information, Figures S11–S13.

85.33(12)° and 94.80(12)° and between 178.3(2)° and 180° (Supporting Information, Table S7–S9). Each metal(II) cation is linked by pairs of μ-1,3-bridging thiocyanato anions into chains (Figure 2). The metal–metal separation within these chains amounts to 5.5861(4) Å for **3-Ni/I**, 5.5738(11) Å for **3-Ni/II**, and 5.7737(4) Å for **3-Mn/III**. The shortest interchain distances are 10.5105(9) Å in **3-Ni/I**, 8.5959(13) Å in **3-Ni/II**, and 8.5647(6) Å in **3-Mn/III**.

Investigations on the Stability of the 1:4 Modifications. In order to determine which of the two Mn modifications is thermodynamically more stable in room temperature conditions, solvent mediated conversion experiments were performed. Saturated solutions of a mixture of **1-Mn/III** and **1-Mn/IV** with additional crystalline powder were stirred for a prolonged time, and afterward the residue was investigated by XRPD (Figure 3). After 5 days, form **IV**

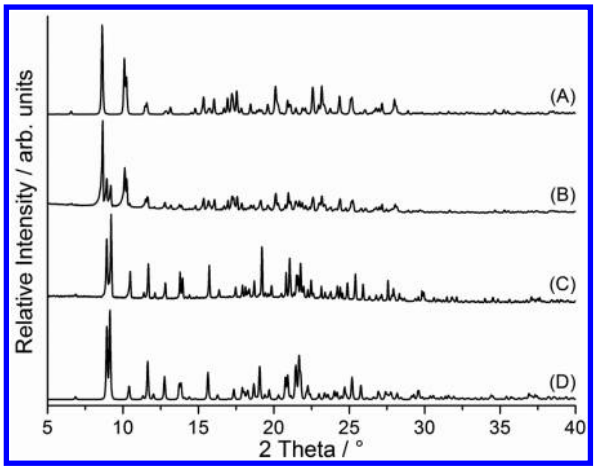

Figure 3. Calculated powder patterns of **1-Mn/IV** (A) and **1-Mn/III** (D), together with the experimental X-ray powder pattern of the mixture of **1-Mn/III** and **1-Mn/IV** (B) and the pattern obtained after stirring this mixture for 5 days in water (C).

disappeared, clearly proving that form **III** is thermodynamically more stable and strongly indicating that **1-Mn/IV** is obtained by kinetic control in the solution based synthesis (Table 1).

For the previously published polymorphs **I** and **II** of Ni, no solvent mediated conversion experiments were performed because in our polymorph screening experiments using different solvents only **1-Ni/II** was obtained, indicating that

dx.doi.org/10.1021/cg500037d | *Cryst. Growth Des.* 2014, 14, 1902–1913

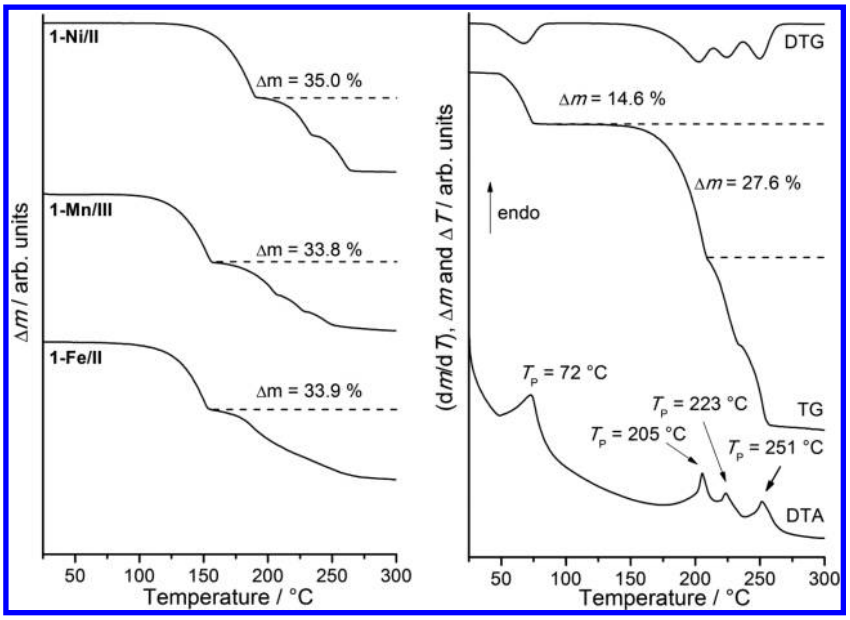

Figure 4. TG curves of **1-Ni/II**, **1-Mn/III**, and **1-Fe/II** (left) and DTG, TG, and DTA curves of **2-Mn** (right). Heating rate = 4 °C/min; Δm = mass loss [%], T_P = peak temperature [°C].

this polymorph is the thermodynamically more stable form at room temperature. As previously mentioned, only a few crystals of **1-Fe/I** were accidently obtained in a mixture with **1-Fe/II**. On storage, these crystals transformed rapidly into **1-Fe/II**, proving that (as for Ni) form **II** is also the thermodynamically stable form at room temperature.

Thermoanalytical Investigations. The thermal properties of the 1:4 compounds **1** and of **2-Mn** were investigated by simultaneous differential thermoanalysis and thermogravimetry (DTA-TG), differential scanning calorimetry (DSC), and temperature-dependent X-ray powder diffraction (HT-XRPD).

On heating to 300 °C, compounds **1-Ni/II**, **1-Mn/III**, **1-Fe/II**, and **2-Mn** exhibited several mass reductions in the TG curve, accompanied by endothermic events in the DTA curves (Figure 4 and Supporting Information, Figure S15). For compounds **1**, the experimental mass loss during the first TG step is in a good agreement with the calculated mass loss for the removal of half of the 4-ethylpyridine ligands, whereas in the second step only one of the ligands is lost (Table 5). The

Table 5. Experimental and Calculated Mass Loss for 1-Ni/II, 1-Mn/III, 1-Fe/II, and 2-Mn

	1-Ni/II	1-Mn/III	1-Fe/II	2-Mn
Δm_{exp} (1st step)	35.0	33.8	33.9	14.6
Δm_{calc}	35.4	35.6	35.6	8.50
Δm_{exp} (2nd step)	17.4	15.0	18.1	27.6
Δm_{calc}	17.7	17.8	17.8	25.5

experimental mass change of Δm_{exp} = 14.6% in the first step of **2-Mn** is in agreement with the loss of two water molecules, and in the second step, half of the 4-ethylpyridine ligands evaporate. On further heating, the remaining ligands are removed, leading to the formation of the metal(II) thiocyanates, which subsequently decompose. Based on these observations, it can be assumed that all of them decompose into compounds of composition $M(NCS)_2(4\text{-ethylpyridine})_2$ in the first step. These might transform into 1:1 compounds of composition $M(NCS)_2(4\text{-ethylpyridine})$ during the second step.

To verify the composition of these intermediates, the TG measurements were stopped after the first weight loss step, and the residues were investigated by XRPD, elemental analysis, and IR spectroscopy. IR spectroscopy indicates that the metal cations are linked by μ-1,3-bridging thiocyanato anions (Supporting Information, Figure S16).

XRPD measurements reveal that the residues obtained in the first heating step of **1-Ni/II**, **1-Mn/III**, and **1-Fe/II** are isotypic and correspond to the structure of **3-Ni/II**, a compound already obtained in solution (Figure 5, top).

Interestingly, in the case of Fe, a new compound of composition $Fe(NCS)_2(4\text{-ethylpyridine})_2$ (**3-Fe/II**) was obtained, for which there is no evident access using solution-based synthesis methods. Similarly, the thermal decompositions of **1-Mn/III** leads to the formation of the corresponding polymorph **II** (**3-Mn/II**), which also was not obtained during the solution-based synthesis. The crystal structures of these forms were obtained by the Rietveld method (Table 2 and Supporting Information, Figure S17–S18).

However, the experimental X-ray powder pattern of the residue obtained in the first TG step of the aqua complex 2-Mn shows that a mixture of modification **II** and **III** of $Mn(NCS)_2(4\text{-ethylpyridine})_2$ has formed (Figure 5, bottom). According to a two-phase Rietveld refinement, 3-Mn/**II** and 3-Mn/**III** have formed in ratio 26.4:73.6 (Supporting Information, Figure S19).

The residues obtained in the second TG step of **1-Mn/III**, **1-Fe/II**, and **2-Mn** gave amorphous XRPD patterns. The residue obtained by thermal decomposition of **1-Ni/II**, however, was of good crystallinity. Moreover, no reflections of the 1:2 compound and of $Ni(NCS)_2$ are present, and the elemental analysis is in agreement with that calculated for the composition $Ni(NCS)_2(4\text{-ethylpyridine})$ (**4-Ni**, Figure 6).

This is further supported by the fact that different batches of this compound show identical XRPD patterns (Supporting Information, Figure S20). Unfortunately all attempts to index this pattern failed, and we cannot exclude that small amounts of a second phase are present. However, the magnetic measurements gave no hints of contaminations. However, in the IR

dx.doi.org/10.1021/cg500037d | Cryst. Growth Des. 2014, 14, 1902–1913

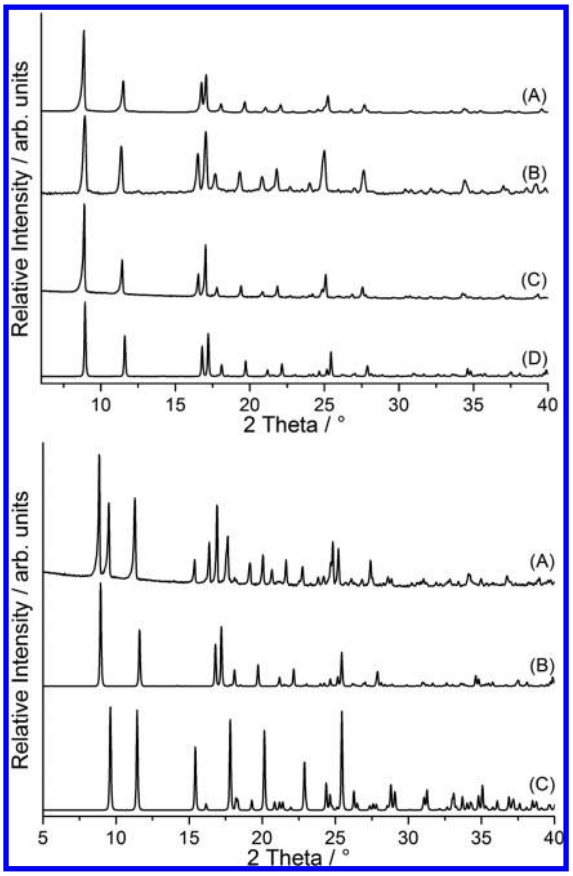

Figure 5. Experimental XRPD patterns of the residues obtained after the first TG step of **1-Ni/II** (A), **1-Mn/III** (B), **1-Fe/II** (C), and **3-Ni/II** (D) calculated from single crystal data (top) and **2-Mn** (A), **3-Mn/III** (B), and **3-Mn/II** (C) calculated from single crystal data (bottom).

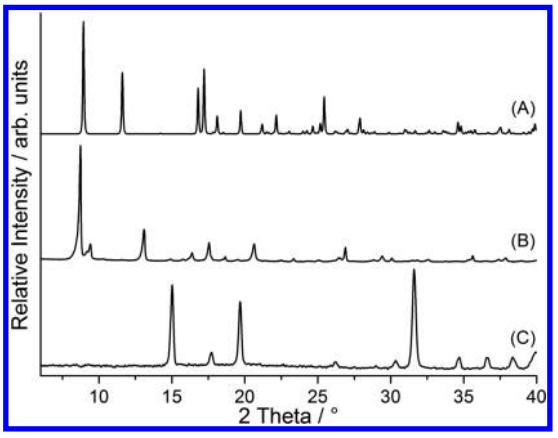

Figure 6. Experimental XRPD of the residues obtained after the second TG step of **1-Ni/II** (B) together with the powder pattern for **3-Ni/II** (A) and $Ni(NCS)_2$ (C).

spectrum of this compound, the ν_{as}(CN) stretching vibration is observed at 2139 and 2117 cm^{-1} (Supporting Information, Figure S20). These values are in agreement with the presence of μ-1,1,3-bridging thiocyanato anions and indicates that a more condensed 1D network has formed, which should be similar to that in $[Cd(NCS)_2(4\text{-ethylpyridine})]_n$ (ν_{as}(CN) = 2124 and 2107 cm^{-1}) and $[Cd(NCS)_2(pyridine)]_n$ (ν_{as}(CN) = 2120 and 2105 cm^{-1}) reported recently (Supporting Information, Figure S21).[81]

To investigate the thermal properties of compounds **1** in greater detail and to check for polymorphic transformations not detected by the DTA investigations, DSC and temperature dependent XRPD measurements were performed.

The DSC curve of **1-Mn/III** is characterized by several endothermic events, observed up to 250 °C (Figure 7). There

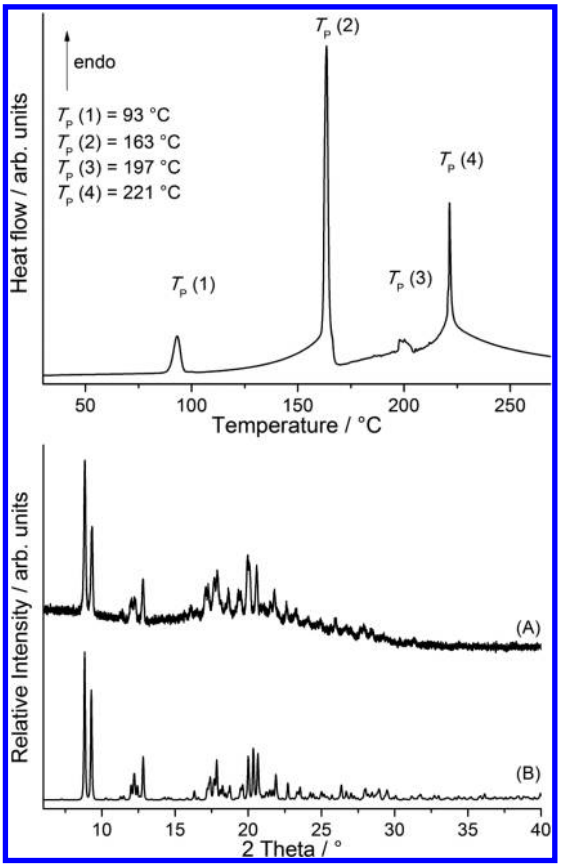

Figure 7. DSC curve for **1-Mn/III** (heating rate of 10 °C/min, T_P = peak temperature in °C) (top) and **1-Ni/I** retrieved from literature (bottom).

is one additional less intense signal at about 93 °C, not visible in the DTA curves. The XRPD investigations clearly prove that this event corresponds to a transformation into a new form (**1-Mn/I**) that was not obtained by crystallization from solution and that is isotypic to **1-Ni/I** and **1-Fe/I** (Figure 7).

Accordingly, it can be concluded that **1-Mn/I** becomes stable at higher temperatures, and because the transition is endothermic, form **I** and form **III** are supposed to behave enantiotropically. On further heating, transformation into 4-ethylpyridine deficient compound $Mn(NCS)_2(4\text{-ethylpyridine})_2$ (**3-Mn/II**) is observed at 163 °C (Figure 4 and Supporting Information, Figure S22). Additional DSC signals at higher temperatures (197 and 221 °C) correspond to a transformation into new amorphous phases. These results are in agreement with the temperature dependent XRPD measurements, which show that **1-Mn/III** transforms into **3-Mn/II** via **1-Mn/I** as an intermediate (Supporting Information, Figure S23). However, in contrast to our DTA-TG and DSC measurements, additional crystalline phases are formed at higher temperatures (Supporting Information, Figure S22).

The DSC measurements of **1-Fe/II** gave no hints for transformation into a new modification but only decomposition

dx.doi.org/10.1021/cg500037d | *Cryst. Growth Des.* 2014, 14, 1902−1913

into $[Fe(NCS)_2(4\text{-ethylpyridine})_2]_n$ (**3-Fe/II**, as already observed in the DTA-TG measurements (Supporting Information, Figure S23)). It should be noted that crystalline **3-Fe/II** was not detected in our HT-XRPD measurements of **1-Fe/II** because this compound directly decomposes into an amorphous phase. However, the formation of either a crystalline or an amorphous phase is not surprising, given that the outcome of such thermoanalytical measurements depends on a number of parameters like the heating rate and the atmosphere used in the experiment.

The DSC measurements on **1-Ni/II** show transformation into **1-Ni/I**, indicating that the latter modification becomes more stable at higher temperatures (Supporting Information, Figure S24). This is in agreement with our investigations on the corresponding Mn modification, **1-Mn/III**. On further heating, **1-Ni/I** transforms into **4-Ni** via **3-Ni/II** as intermediate, as already observed in the DTA-TG measurements. Similar results were obtained by the HT-XRPD measurements. Surprisingly, small differences are found in the powder pattern of **4-Ni** obtained by the DTA-TG and DSC measurements and the one measured by HT-XRPD at about 270 °C. These differences cannot be traced back to an anisotropic shift of the lattice parameters because when the phase observed at high temperatures is measured afterward at room temperature the differences are still present. A high-temperature phase transition of **4-Ni** can also be excluded; when this compound is investigated by HT-XRPD measurements, it decomposes directly into $Ni(NCS)_2$ without any previous transformation. Therefore, obviously a new high temperature phase has formed in the XRPD measurements that is not observed in the DTA-TG and DSC measurements.

Investigations on the Stability of 3-Ni/I and 3-Ni/II. Numerous synthesis trials showed that almost always **3-Ni/II** is obtained in solution. Surprisingly, a few single crystals of a second polymorph, **3-Ni/I**, were accidently obtained. In order to check whether **3-Ni/I** is formed by kinetic control and is supposed to transform into **3-Ni/II**, nickel(II) thiocyanate and 4-ethylpyridine were stirred in ratio 1:2 in water, and the residues obtained were investigated by XRPD as a function of time. At early stages, the solution become deep blue colored, and 1:4 compound **1-Ni/II** was formed. Afterward, transformation into a light blue colored crystalline powder of **3-Ni/I** is observed, which transformed into a light green colored crystalline powder of **3-Ni/II**. It can be concluded that **3-Ni/II** represents the thermodynamically stable form at room temperature (Figure 8). Additionally, DSC and temperature dependent XRPD measurements on **3-Ni/I** and **3-Ni/II** gave no hints for polymorphic transformations.

Investigations on the Stability of 3-Mn/II and 3-Mn/III. To prove which of the two different 1:2 modifications, **3-Mn/II** or **3-Mn/III**, represents the thermodynamically most stable form at room-temperature, a solvent mediated conversion experiment was performed. Mixture of **3-Mn/II** and **3-Mn/III** was stirred in a saturated solution in ethanol at room temperature for 3 days. Afterward, the residues were filtered and investigated by XRPD. It was shown that **3-Mn/II** transforms into **3-Mn/III**, which is the thermodynamically stable form (Figure 9). Additional DSC and XRPD measurements on forms **3-Mn/II** and **3-Mn/III** gave no hint for additional polymorphic transformations.

Thermodynamic Relations and Transformations between All Compounds. In the investigations presented above, several compounds of composition $M(NCS)_2(4\text{-ethylpyridine})_4$ and $[M(NCS)_2(4\text{-ethylpyridine})_2]_n$ were obtained, crystallizing in different modifications. On stirring, transformation of **1-Mn/III** into the thermodynamically more stable form **1-Mn/IV** is observed (Figure 10). **1-Mn/III** is also formed as an intermediate in the solution based synthesis and, therefore, is clearly metastable at room temperature. On heating **1-Mn/III**, a polymorphic endothermic transformation into **1-Mn/I** is observed, proving that the latter is more stable at higher temperatures and that both forms behave enantiotropically. Surprisingly, for Mn and Ni, form **I** is already obtained at room temperature, but it is metastable and transforms into the stable form **II**, which was not obtained for Mn (Figure 10). It should be noted that on heating **1-Ni/II**

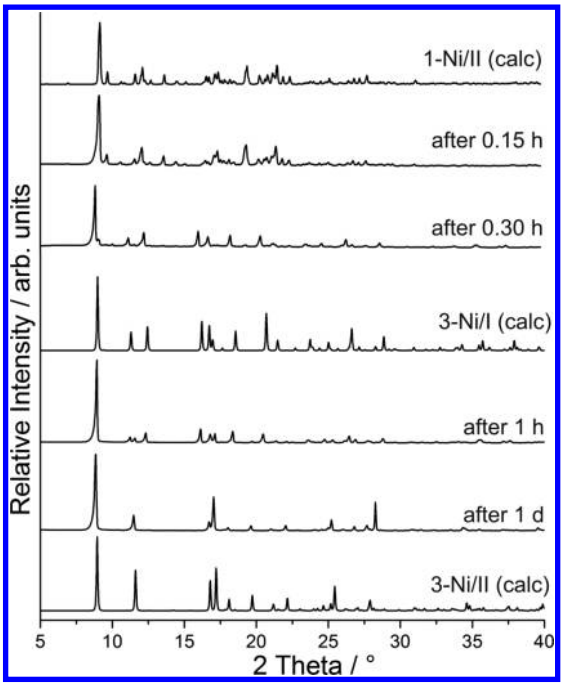

Figure 8. Calculated powder pattern of compound **1-Ni/II**, together with the experimental X-ray powder patterns when $Ni(NCS)_2$ is reacted with 4-ethylpyridine in water for 0.15 and 0.30 h and calculated XRPD pattern of **3-Ni/I** and experimental XRPD patterns of the sample stirred for 1 h and 1 d in water together with the calculated pattern for **3-Ni/II**.

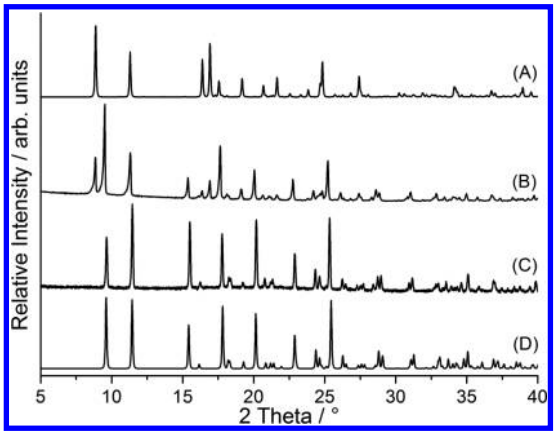

Figure 9. Calculated powder patterns from Rietveld refinement of **3-Mn/II** (A), mixture of **3-Mn/II** and **3-Mn/III** (B), and mixture stirred for 3 days in ethanol (C), together with the calculated powder pattern of **3-Mn/III** (D).

dx.doi.org/10.1021/cg500037d | Cryst. Growth Des. 2014, 14, 1902−1913

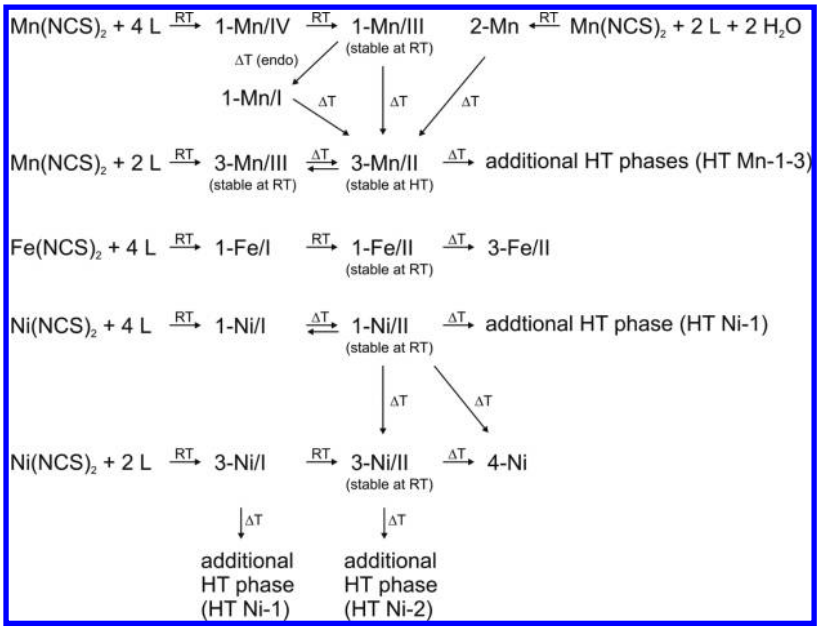

Figure 10. Schematic representation of the thermodynamic relations and the transition behavior of all compounds.

Table 6. Results of the Magnetic Measurements on the 4-Ethylpyridine-Deficient 1:2 Compounds 3-Ni/I, 3-Ni/II, 3-Mn/II, 3-Mn/III, and 3-Fe/II at H_{DC} = 1 kOe

	3-Ni/I	3-Ni/II	3-Fe/II	3-Mn/II	3-Mn/III
$T_{ordering}$, K				T_N = 21.5 K	T_N = 23.9 K
C, cm^3 K mol^{-1}	1.17	1.12	2.90	3.35	4.88
θ, K	4.6	3.9	−1.6	−36.1	−39.2
μ_{eff}(exp)/μ_B	3.06	2.97	4.77	4.87	5.83
μ_{eff}(calc)/μ_B (hs)	2.82	2.82	4.89	5.92	5.92
fit region, K	2−300	2−300	2−300	50−300	2−300

transforms into **1-Ni/I** in an endothermic reaction; therefore both forms behave enantiotropically with form **I** being stable at higher temperatures, as was the case for Mn.

On heating of **1-Mn/III**, **1-Fe/II**, and **1-Ni/II**, half of the ligands are removed and transformations into new compounds of composition M(NCS)$_2$(4-ethylpyridine)$_2$ are observed. In those cases, all compounds are isotypic and crystallize as form **3-M/II** (Figure 10). Further experiments, however, show that for Mn this crystalline phase is only stable at higher temperatures, whereas at room temperature and in solution it transforms to **3-Mn/III**. In the case of Fe, this 4-ethylpyridine deficient compound cannot be obtained from solution, whereas for Ni, form **II** represents the thermodynamically stable form already at room temperature. As it can be seen, the 4-ethylpyridine deficient modifications of Mn and Ni behave differently.

It should be noted that for Ni a second polymorph (**3-Ni/I**) exists that is metastable at room temperature and transforms into the stable form **3-Ni/II** (Figure 10). However, at higher temperature, additional crystalline phases are observed whose structures are still unknown.

Magnetic Investigations. For compounds **1-Ni/II**, **1-Mn/III**, **1-Mn/IV**, **1-Fe/II**, and **2-Mn**, the temperature dependence of the susceptibility was investigated in the temperature range of 300−2 K applying a magnetic field of H_{DC} = 1 kOe, and for all compounds, a simple Curie−Weiss paramagnetic behavior without any anomaly was observed (Supporting Information, Figure S25). Upon analysis of the magnetic data according to the Curie−Weiss law, $\chi_M = C/(T - \theta)$ yields a Weiss constant of θ = 3.4 K for **1-Ni/II**, θ = 0.1 K for **1-Mn/III**, θ = −0.9 K for **1-Fe/II**, θ = −0.38 K for **2-Mn**, and θ = −35.0 K for **1-Mn/IV**, indicating relatively strong antiferromagnetic interactions for the latter (Supporting Information, Table S10).

Surprisingly, a similar behavior is observed for **3-Ni/I** and **3-Ni/II**, even though in these compounds the cations are linked by μ-1,3-bridging thiocyanato anions (Supporting Information, Figure S25). Fitting the magnetic data according to the Curie−Weiss law lead to a Weiss constant of θ = 4.6 K for **3-Ni/I** and θ = 3.9 K for **3-Ni/II**, indicating weak ferromagnetic interactions (Table 6). For **3-Fe/II**, a similar behavior was found, and θ was determined to be 1.6 K (Table 6 and Supporting Information, Figure S25).

In contrast, for **3-Mn/II**, a sharp maximum is observed in the χ_M versus T curve indicating antiferromagnetic ordering at T_N = 21.5 K (Figure 11, top). The same behavior is found for **3-Mn/III**, but T_N is shifted slightly to 23.9 K (Figure 11, bottom). Fitting the magnetic data according to the Curie−Weiss law yields a strong negative Weiss constant of θ = −36.1 K for **3-Mn/II** and of −39.2 K for **3-Mn/III** indicating relatively strong antiferromagnetic interactions (Table 6). To check for metamagnetic behavior, initial curves at 2 K up to 90 kOe were measured, which show a behavior typical for antiferromagnets in the case of **3-Mn/II** and **3-Mn/III** (Supporting Information, Figure S26).

Magnetic measurement on **4-Ni** at H_{DC} = 1 kOe showed antiferromagnetic ordering at T_N = 8.1 K (Figure 12). Fitting the magnetic data according to the Curie−Weiss law yields to a strong positive Weiss constant of θ = 30.3 K. From the

dx.doi.org/10.1021/cg500037d | Cryst. Growth Des. 2014, 14, 1902−1913

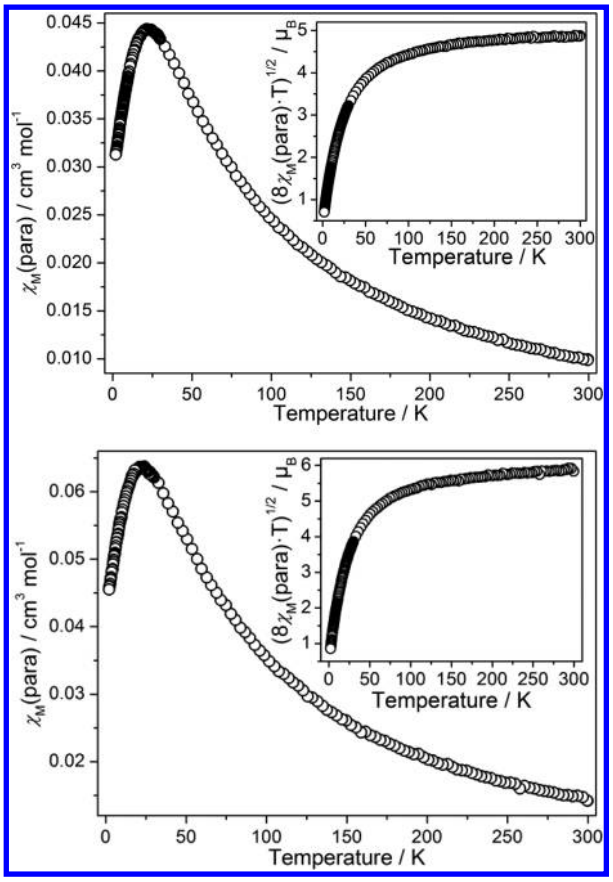

Figure 11. χ_M and $(8\chi_M T)^{1/2}$ (inset) as a function of temperature at H_{DC} = 1 kOe for **3-Mn/II** (top) and **3-Mn/III** (bottom).

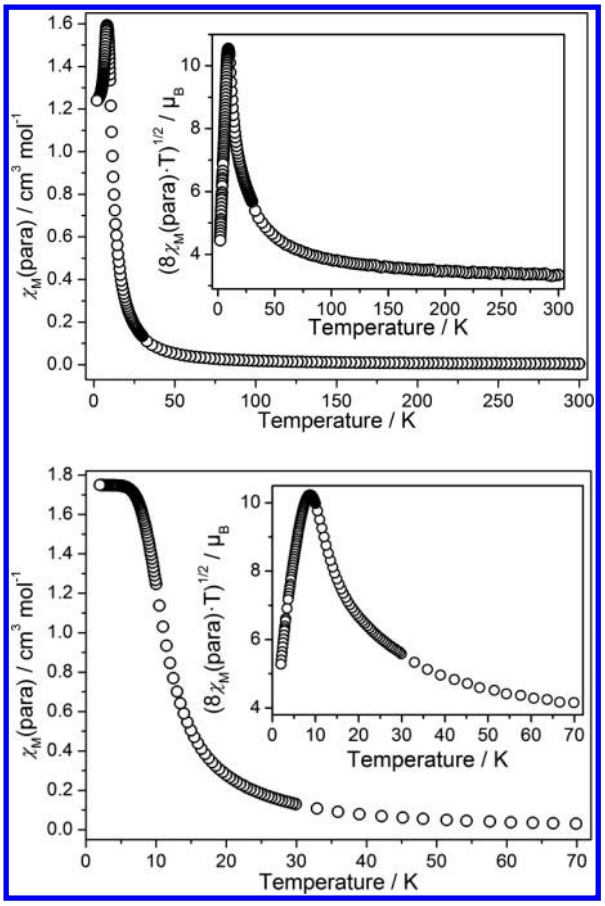

Figure 12. χ_M and $(8\chi_M T)^{1/2}$ (inset) as a function of temperature at H_{DC} = 1 kOe (top) and H_{DC} = 2 kOe (bottom) for **4-Ni**.

$(8\chi_M T)^{1/2}$ vs T curve, a room-temperature value of the effective magnetic moment of $\mu_{eff}(exp) = 3.34\mu_B$ was obtained, which is agreement with the spin-only value for Ni^{2+} (S = 1, g = 2). On cooling, an increase in the $\chi_M T$ curve is observed indicative of ferromagnetic interactions between the nickel(II) cations, and on further cooling, this curve drops dramatically (Supporting Information, Figure S27).

Magnetization measurements at 2 K in the range of 0−90 kOe show a sigmoidal shape indicative of metamagnetic behavior (Supporting Information, Figure S28). From the first derivative of the initial curve, the critical field, H_C, was determined as 1.4 kOe. A magnetization loop experiment at 2 K in the range ±10 kOe showed a small hysteresis (Figure 13).

Temperature dependent magnetic measurement above the critical field was performed at H_{DC} = 2 kOe, which clearly shows the transition into a saturated paramagnetic phase. The ordering temperature of T_C = 10.0 K was obtained from the first derivative of the susceptibility curve. To analyze the saturated paramagnetic phase in more detail, ZFC/FC (zero-field cooled/field-cooled) measurements were performed, in which a small splitting typically for ferromagnetic behavior can be observed (Supporting Information, Figure S29). Further M versus H measurements at different temperatures below the antiferromagnetic ordering temperature and temperature dependent measurements at different magnetic fields below the critical fields were combined to prepare the phase diagram, which is typical for a metamagnet (Figure 14 and Figures S30−S31 in the Supporting Information).[82−84]

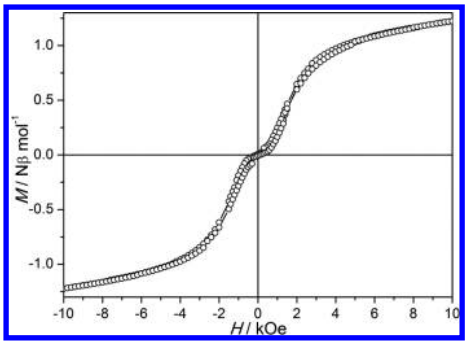

Figure 13. Magnetization loop at T = 2 K in range the ±10 kOe for **4-Ni**.

CONCLUSIONS

In the present contribution, a large number of new coordination compounds based on transition metal thiocyanates and 4-ethylpyridine as coligand are reported. Several of them crystallize in different polymorphic modifications. Interestingly, for the compounds of composition $M(NCS)_2(L)_4$, Fe and Ni have the same structure in the thermodynamically stable form at room-temperature, whereas the one with Mn prefers a different structural arrangement. For the compounds of composition $M(NCS)_2(L)_2$, however, only one common modification is found, which is thermodynamically stable for Ni but metastable for Mn. This nicely demonstrates that even for such simple compounds, where normally isotypic structures are expected, several polymorphic

dx.doi.org/10.1021/cg500037d | Cryst. Growth Des. 2014, 14, 1902−1913

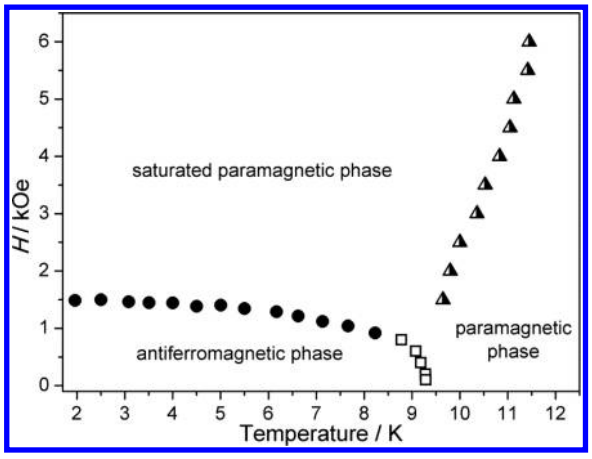

Figure 14. Magnetic phase diagram, maximum as determined from the first derivative of dM/dH versus H at different temperatures (●) and from the maximum of the molar paramagnetic susceptibility at different magnetic fields.

modifications can be found. Additionally, some new metastable forms were detected by thermal decomposition of suitable precursor compounds. One Fe compound was obtained by the solid state route, and it was shown that it cannot be prepared in solution, which shows the high potential of this alternative solid state, decomposition based, synthetic approach. Moreover, on thermal decomposition, a further compound of unusual stoichiometry is observed for which a more condensed 1D structure is expected. Unfortunately the structure of this compound is still unknown, and because the pattern cannot be indexed, it cannot be excluded that a small amount of contamination or a second modification is present. From our magnetic investigations, there is no hint of paramagnetic contamination, which would be clearly visible in the antiferromagnetic phase. However, magnetic measurements reveal that it is a metamagnet, and it can be expected that the antiferromagnetic interactions are mediated by the metal thiocyanato chains. For the two modifications of manganese with μ-1,3-bridging anions antiferromagnetism is observed with similar ordering temperatures. Finally, as expected, all compounds with only terminal N-bonded thiocyanato anions show simple Curie–Weiss paramagnetism without magnetic anomalies, and thus μ-1,3-bridging compounds must be prepared if cooperative magnetic properties should be generated.

■ ASSOCIATED CONTENT

Supporting Information

Experimental details on the synthesis, the structures, and the characterization including IR-spectra, DSC curves, X-ray powder pattern, and magnetic measurements. This material is available free of charge via the Internet at http://pubs.acs.org.

■ AUTHOR INFORMATION

Corresponding Author

*Email: cnaether@ac.uni-kiel.de. Fax: +49 880 1520. Tel: +49 880 2092.

Notes

The authors declare no competing financial interest.

■ ACKNOWLEDGMENTS

This project was supported by the Deutsche Forschungsgemeinschaft (Project No. Na 720/3-1) and the State of Schleswig-Holstein. We thank Prof. Dr. Wolfgang Bensch for access to his experimental facilities. Special thanks to Inke Jess for the single crystal measurements and to Maren Rasmussen and Henning Lühmann for the magnetic measurements.

■ REFERENCES

(1) Janiak, C. *Dalton Trans.* **2003**, 2781–2804.
(2) James, S. L. *Chem. Soc. Rev.* **2003**, *32*, 276–288.
(3) Maspoch, D.; Ruiz-Molina, D.; Veciana, J. *Chem. Soc. Rev.* **2007**, *36*, 770–818.
(4) Li, H.; Eddaoudi, M.; O'Keeffe, M.; Yaghi, O. M. *Nature* **1999**, *402*, 276–279.
(5) Kitagawa, S.; Uemura, K. *Chem. Soc. Rev.* **2005**, *34*, 109–119.
(6) Hagrman, P. J.; Hagrman, D.; Zubieta, J. *Angew. Chem., Int. Ed.* **1999**, *38*, 2638–2684.
(7) Braga, D.; Maini, L.; Polito, M.; Scaccianoce, L.; Cojazzi, G.; Grepioni, F. *Coord. Chem. Rev.* **2001**, *216*, 225–248.
(8) Moulton, B.; Zaworotko, M. J. *Curr. Opin. Solid State Mater. Sci.* **2002**, *6*, 117–123.
(9) Aakeroy, C. B.; Champness, N. R.; Janiak, C. *CrystEngComm* **2010**, *12*, 22–43.
(10) Desiraju, G. R. *Crystal Engineering - The Design of Organic Solids*; Elsevier: Amsterdam - Oxford - New York - Tokyo, 1989.
(11) Desiraju, G. R. *Organic Solid State Chemistry*; Studies in Organic Chemistry, Vol. *32*; Elsevier: Amsterdam - Oxford - New York - Tokyo, 1987.
(12) Aakeröy, C. B.; Seddon, K. R. *Chem. Soc. Rev.* **1993**, *22*, 397–407.
(13) Zaworotko, M. J. *Chem. Soc. Rev.* **1994**, *23*, 283–288.
(14) Desiraju, G. R. *Chem. Commun.* **1997**, 1475–1482.
(15) Braga, D.; Grepioni, F.; Desiraju, G. R. *Chem. Rev.* **1998**, *98*, 1375–1406.
(16) Blake, A. J.; Champness, N. R.; Hubberstey, P.; Li, W.-S.; Withersby, M. A.; Schröder, M. *Coord. Chem. Rev.* **1999**, *183*, 117–138.
(17) Sharma, C. V. K. *Cryst. Growth Des.* **2002**, *2*, 465–474.
(18) Brammer, L. *Chem. Soc. Rev.* **2004**, *33*, 476–489.
(19) Rovira, C.; Veciana, J. *CrystEngComm* **2009**, *11*, 2031–2031.
(20) Zaworotko, M. J. *Nat. Chem.* **2011**, *3*, 653–653.
(21) Blake, A. J.; Brooks, N. R.; Champness, N. R.; Crew, M.; Gregory, D. H.; Hubberstey, P.; Schröder, M.; Deveson, A.; Fenske, D.; Hanton, L. R. *Chem. Commun.* **2001**, 1432–1433.
(22) Braga, D.; Grepioni, F. *Chem. Soc. Rev.* **2000**, *29*, 229–238.
(23) Wöhlert, S.; Boeckmann, J.; Jess, I.; Näther, C. *CrystEngComm* **2012**, *14*, 5412–5420.
(24) Näther, C.; Wriedt, M.; Jeß, I. *Inorg. Chem.* **2003**, *42*, 2391–2397.
(25) Näther, C.; Jeß, I. *Inorg. Chem.* **2003**, *42*, 2968–2976.
(26) Näther, C.; Bhosekar, G.; Jeß, I. *Inorg. Chem.* **2007**, *46*, 8079–8087.
(27) Näther, C.; Jeß, I.; Lehnert, N.; Hinz-Hübner, D. *Solid State Sci.* **2003**, *5*, 1343–1357.
(28) Tao, J.; Wei, R.-J.; Huang, R.-B.; Zheng, L.-S. *Chem. Soc. Rev.* **2012**, *41*, 703–737.
(29) Wang, C.-F.; Zhu, Z.-Y.; Zhou, X.-G.; Weng, L.-H.; Shen, Q.-S.; Yan, Y.-G. *Inorg. Chem. Commun.* **2006**, *9*, 1326–1330.
(30) Robin, A. Y.; Fromm, K. M. *Coord. Chem. Rev.* **2006**, *250*, 2127–2157.
(31) Barnett, S. A.; Blake, A. J.; Champness, N. R.; Wilson, C. *Chem. Commun.* **2002**, 1640–1641.
(32) Moulton, B.; Zaworotko, M. J. *Chem. Rev.* **2001**, *101*, 1629–1658.
(33) Zeng, Y.-F.; Hu, X.; Liu, F.-C.; Bu, X.-H. *Chem. Soc. Rev.* **2009**, *38*, 469–480.
(34) Kurmoo, M. *Chem. Soc. Rev.* **2009**, *38*, 1353–1379.

(35) Maspoch, D.; Ruiz-Molina, D.; Veciana, J. *J. Mater. Chem.* **2004**, *14*, 2713−2723.
(36) Zhang, S.-Y.; Shi, W.; Lan, Y.; Xu, N.; Zhao, X.-Q.; Powell, A. K.; Zhao, B.; Cheng, P.; Liao, D.-Z.; Yan, S.-P. *Chem. Commun.* **2011**, *47*, 2859−2861.
(37) Sun, H.-L.; Wang, Z.-M.; Gao, S. *Coord. Chem. Rev.* **2010**, *254*, 1081−1100.
(38) Vallejo, J.; Cano, J.; Castro, I.; Julve, M.; Lloret, F.; Fabelo, O.; Canadillas-Delgado, L.; Pardo, E. *Chem. Commun.* **2012**, *48*, 7726−7728.
(39) Létard, J.-F.; Asthana, S.; Shepherd, H. J.; Guionneau, P.; Goeta, A. E.; Suemura, N.; Ishikawa, R.; Kaizaki, S. *Chem.—Eur. J.* **2012**, *18*, 5924−5934.
(40) Zhang, X.-H.; Hao, Z.-M.; Zhang, X.-M. *Chem.—Eur. J.* **2011**, *17*, 5588−5594.
(41) Gil-Hernandez, B.; Maclaren, J. K.; Hoppe, H. A.; Pasan, J.; Sanchiz, J.; Janiak, C. *CrystEngComm* **2012**, *14*, 2635−2644.
(42) Gil-Hernández, B.; Gili, P.; Vieth, J. K.; Janiak, C.; Sanchiz, J. *Inorg. Chem.* **2010**, *49*, 7478−7490.
(43) Shurdha, E.; Lapidus, S. H.; Stephens, P. W.; Moore, C. E.; Rheingold, A. L.; Miller, J. S. *Inorg. Chem.* **2012**, *51*, 9655−9665.
(44) Wriedt, M.; Sellmer, S.; Näther, C. *Inorg. Chem.* **2009**, *48*, 6896−6903.
(45) Wriedt, M.; Sellmer, S.; Näther, C. *Dalton Trans.* **2009**, 7975.
(46) Wriedt, M.; Jeß, I.; Näther, C. *Eur. J. Inorg. Chem.* **2009**, 1406−1413.
(47) Adams, C. J.; Muñoz, M. C.; Waddington, R. E.; Real, J. A. *Inorg. Chem.* **2011**, *50*, 10633−10642.
(48) Adams, C. J.; Real, J. A.; Waddington, R. E. *CrystEngComm* **2010**, *12*, 3547−3553.
(49) Tao, J.-Q.; Gu, Z.-G.; Wang, T.-W.; Yang, Q.-F.; Zuo, J.-L.; You, X.-Z. *Inorg. Chim. Acta* **2007**, *360*, 4125−4132.
(50) Shi, J. M.; Chen, J. N.; Wu, C. J.; Ma, J. P. *J. Coord. Chem.* **2007**, *60*, 2009−2013.
(51) Real, J. A.; De Munno, G.; Munoz, M. C.; Julve, M. *Inorg. Chem.* **1991**, *30*, 2701−2704.
(52) Adams, C. J.; Haddow, M. F.; Harding, D. J.; Podesta, T. J.; Waddington, R. E. *CrystEngComm* **2011**, *13*, 4909−4914.
(53) Näther, C.; Wöhlert, S.; Boeckmann, J.; Wriedt, M.; Jeß, I. *Z. Anorg. Allg. Chem.* **2013**, *639*, 2696−2714.
(54) Nesterova, O. V.; Petrusenko, S. R.; Kokozay, V. N.; Skelton, B. W.; Jezierska, J.; Linert, W.; Ozarowski, A. *Dalton Trans.* **2008**, 1431−1436.
(55) González, R.; Acosta, A.; Chiozzone, R.; Kremer, C.; Armentano, D.; De Munno, G.; Julve, M.; Lloret, F.; Faus, J. *Inorg. Chem.* **2012**, *51*, 5737−5747.
(56) Machura, B.; Palion, J.; Penkala, M.; Groń, T.; Duda, H.; Kruszynski, R. *Polyhedron* **2013**, *56*, 189−199.
(57) Banerjee, S.; Drew, M. G. B.; Lu, C.-Z.; Tercero, J.; Diaz, C.; Ghosh, A. *Eur. J. Inorg. Chem.* **2005**, *2005*, 2376−2383.
(58) Ma, Q.; Zhu, M.; Lu, L.; Feng, S.; Yan, J. *Inorg. Chim. Acta* **2011**, *370*, 102−107.
(59) Näther, C.; Greve, J. *J. Solid State Chem.* **2003**, *176*, 259−265.
(60) Wriedt, M.; Näther, C. *Chem. Commun.* **2010**, *46*, 4707−4709.
(61) Näther, C.; Jeß, I. *J. Solid State Chem.* **2002**, *169*, 103−112.
(62) Adams, C. J.; Kurawa, M. A.; Lusi, M.; Orpen, A. G. *CrystEngComm* **2008**, *10*, 1790−1795.
(63) Adams, C. J.; Crawford, P. C.; Orpen, A. G.; Podesta, T. J.; Salt, B. *Chem. Commun.* **2005**, 2457−2458.
(64) James, S. L.; Adams, C. J.; Bolm, C.; Braga, D.; Collier, P.; Friscic, T.; Grepioni, F.; Harris, K. D. M.; Hyett, G.; Jones, W.; Krebs, A.; Mack, J.; Maini, L.; Orpen, A. G.; Parkin, I. P.; Shearouse, W. C.; Steed, J. W.; Waddell, D. C. *Chem. Soc. Rev.* **2012**, *41*, 413−447.
(65) Braga, D.; Giaffreda, S. L.; Grepioni, F.; Pettersen, A.; Maini, L.; Curzi, M.; Polito, M. *Dalton Trans.* **2006**, 1249−1263.
(66) Braga, D.; Curzi, M.; Lusi, M.; Grepioni, F. *CrystEngComm* **2005**, *7*, 276−278.
(67) Braga, D.; Curzi, M.; Grepioni, F.; Polito, M. *Chem. Commun.* **2005**, 2915−2917.
(68) Müller-Buschbaum, K. *Z. Anorg. Allg. Chem.* **2005**, *631*, 811−828.
(69) Wöhlert, S.; Näther, C. *Eur. J. Inorg. Chem.* **2013**, *2013*, 2528−2537.
(70) Wöhlert, S.; Wriedt, M.; Fic, T.; Tomkowicz, Z.; Haase, W.; Näther, C. *Inorg. Chem.* **2013**, *52*, 1061−1068.
(71) Wöhlert, S.; Ruschewitz, U.; Näther, C. *Cryst. Growth Des.* **2012**, *12*, 2715−2718.
(72) Wöhlert, S.; Boeckmann, J.; Wriedt, M.; Näther, C. *Angew. Chem., Int. Ed.* **2011**, *50*, 6920−6923.
(73) Boeckmann, J.; Wriedt, M.; Näther, C. *Chem.—Eur. J.* **2012**, *18*, 5284−5289.
(74) Boeckmann, J.; Näther, C. *Chem. Commun.* **2011**, *47*, 7104−7106.
(75) Boeckmann, J.; Näther, C. *Dalton Trans.* **2010**, *39*, 11019−11026.
(76) Boeckmann, J.; Näther, C. *Polyhedron* **2012**, *31*, 587−595.
(77) Wöhlert, S.; Fic, T.; Tomkowicz, Z.; Ebbinghaus, S. G.; Rams, M.; Haase, W.; Näther, C. *Inorg. Chem.* **2013**, *52*, 12947−12957.
(78) Moore, M. H.; Nassimbeni, L. R.; Niven, M. L. *J. Chem. Soc., Dalton Trans.* **1987**, 2125−2140.
(79) Rietveld, H. M. *J. Appl. Crystallogr.* **1969**, *2*, 65−71.
(80) Sheldrick, G. M. *Acta Crystallogr.* **2008**, *A64*, 112−122.
(81) Wöhlert, S.; Jess, I.; Näther, C. *Z. Anorg. Allg. Chem.* **2013**, *639*, 385−391.
(82) Miyasaka, H.; Takayama, K.; Saitoh, A.; Furukawa, S.; Yamashita, M.; Clérac, R. *Chem.—Eur. J.* **2010**, *16*, 3656−3662.
(83) Wang, X.-Y.; Wang, L.; Wang, Z.-M.; Su, G.; Gao, S. *Chem. Mater.* **2005**, *17*, 6369−6380.
(84) Zhang, D.; Wang, H.; Chen, Y.; Ni, Z.-H.; Tian, L.; Jiang, J. *Inorg. Chem.* **2009**, *48*, 11215−11225.